



Universidad Autónoma
de Madrid

Biblos-e Archivo
Repositorio Institucional UAM

Repositorio Institucional de la Universidad Autónoma de Madrid

<https://repositorio.uam.es>

Esta es la **versión de autor** del artículo publicado en:
This is an **author produced version** of a paper published in:

IEEE Transactions on Antennas and Propagation 71.12 (2023): 10032 - 10037

DOI: <https://doi.org/10.1109/TAP.2023.3323759>

Copyright: © 2023 IEEE

El acceso a la versión del editor puede requerir la suscripción del recurso
Access to the published version may require subscription

Communication

Modal Spectrum Shaping and Rotational Unit-Cell Design of Second-Order Symmetric Waveguides

Gines Garcia-Contreras, Juan Córcoles, *Senior Member, IEEE*, and Jorge A. Ruiz-Cruz, *Senior Member, IEEE*

Abstract—In this work we will introduce the role of second-order symmetries in modal spectrum shaping, focusing on structures with discrete rotational symmetry, which are notably useful for applications with dual linear and circular polarization. Relevant examples are provided, as well as a rigorous approach to model the effect that second-order symmetries along with the geometry of the rotational unit cell have on the mode-class monomode bandwidth. Modal spectrum shaping and rotational transversal dispersion diagrams are checked with asymptotic cases and results for regular polygons. Finally, a general workflow for the design of the rotational unit cell is provided.

Index Terms—Higher-order symmetries, Transverse Electric (TE) modes, Transverse Magnetic (TM) modes, waveguides.

I. INTRODUCTION

Communication systems are subject to an ever increasing demand of higher bandwidth, with the objective of improving data rates. This is the case for ultra wide band (UWB) applications [1], or fifth and sixth generation mobile communications [2]. A common approach for achieving this goal is moving to higher frequencies, when spectrum is available. If this is not the case, for waveguide media, a practical approach is using dual polarization [3], [4] and/or modifying the cross-section of the waveguides, displacing higher-order modes to higher frequencies, e.g. using ridge or double ridge waveguides [5], [6]. Extended bandwidth can also be achieved by controlling the excitation of the problem, specifically the symmetry of its electromagnetic field, so that only the modes belonging to certain classes are generated [7]–[9]. Moreover, dual polarization implicitly demands symmetric devices to guarantee no coupling exists between the two first degenerate modes.

The last two procedures are commonly carried out for waveguides having first-order symmetries, which are the classical specular symmetries with respect to a plane. They can also be applied to other higher-order symmetries, such as second-order discrete rotational symmetry w.r.t. an angle of $2\pi/N$, where N is positive integer, called C_N symmetry; or the combination of first- and second-order symmetries, referred to as $C_{N,\nu}$ [10]. Both of these kinds of geometries are present in a variety of devices such as polarizers and field

rotators [11], [12], and have lately regained relevance thanks in part to their interesting dispersion properties [13], [14].

Recently, some formulations have been presented to natively compute C_N and $C_{N,\nu}$ modes in waveguides without any post processing [15]. In this paper we provide various tools to understand how mode-class monomode bandwidth defined for various classes is characterized regardless of the symmetry factor N , generalizing some concepts from [10] and introducing other new ones. A general approach is presented for examining and synthesizing rotational unit cells. It leads to rigorous results, checked with analytical asymptotic cases. Specific data as well as comprehensive rotational transversal dispersion diagrams are presented along with a workflow that can aid in designing rotationally symmetric devices.

II. MODE CLASSES IN DIFFERENT SYMMETRY SCHEMES

Waveguides with second-order (discrete rotational) symmetry C_N [10] are generated through the angular repetition of a rotational unit cell (displayed in orange in Fig. 1). Both cases in Figs. 1(a), (b) can be seen as particular representations of a more general problem, displayed in Fig. 2(a). Although both cross sections in Fig. 1 may seem very different at first glance (for instance only one has first-order symmetry at both planes zx and zy), we will show that it is possible to establish relationships between them through their rotational unit cells.

In homogeneous waveguides enclosed by perfect conductors (the case under study, as shown in Fig. 1), the modal expansion of the electromagnetic field is obtained by solving the scalar Helmholtz equation for a function ψ ($\psi = H_z$ for Transverse Electric (TE) modes, and $\psi = E_z$ for Transverse Magnetic (TM) modes) [16] $\nabla_t^2 \psi + k_c^2 \psi = 0$, where k_c is the cutoff wavenumber, directly related to the cutoff frequency by the relationship $f_c = k_c/(2\pi\sqrt{\mu\epsilon})$.

A. First-Order Symmetry

The first-order boundary conditions are referred to as Perfect Electric Wall (PEW) and Perfect Magnetic Wall (PMW). They are mathematically enforced in an eventual axial symmetry plane C (with normal vector \hat{n}) in the following way:

$$\nabla_t \psi \cdot \hat{n}|_C = 0 \quad \psi|_C = 0 \quad (1)$$

where the leftmost expression in (1) imposes a PEW in TE modes and a PMW in TM modes, and the rightmost expression in (1) imposes a PEW in TM modes and a PMW in TE modes. Crucially, this well known property allows for categorizing the modes into two or four mode classes, depending on the

Manuscript received 23 March, 2023; revised 27 July, 2023. This work was supported by the Spanish Government under grant PID2020-116968RB-C32 (DEWICOM) and TED2021-130650B-C21 (ANT4CLIM) funded by MCIN/AEI/ 10.13039/501100011033 (Agencia Estatal de Investigación) and by UE (European Union) "NextGenerationEU"/PRTR. (Corresponding author: Gines Garcia-Contreras.)

The authors are with the Department of Electronic and Communication Technology, Escuela Politécnica Superior, Universidad Autónoma de Madrid, 28049 Madrid, Spain (e-mail: gines.garcia@uam.es; juan.corcoles@uam.es, jorge.ruizcruz@uam.es).

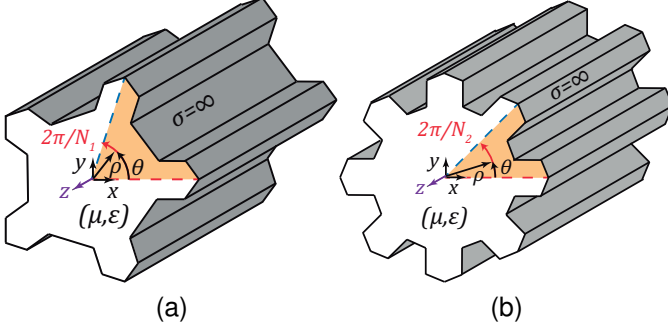


Fig. 1. Homogeneous waveguides with discrete rotational symmetry generated systematically with the rotational unit cell in Fig. 2. (a) $N_1 = 5$, (b) $N_2 = 8$. The waveguide is enclosed by perfect conductor (conductivity $\sigma = \infty$) and filled by homogeneous dielectric permittivity ϵ and magnetic permeability μ .

first-order symmetry type of the waveguide cross-section: one-fold PEW and PMW classes, which will be noted as noted as A and B, respectively, for the sake of simplicity, or two-fold PEW/PEW, PMW/PMW, PEW/PMW, PMW/PEW classes [8], [16], noted in this work as A, B, C and D. If the device is not $C_{N,\nu}$, first-order symmetry does not guarantee that the two first modes in the full spectrum will be degenerate.

B. Second-Order Symmetry

For second-order discrete rotational C_N symmetry, modes can be characterized with a complex-valued eigenfunction ψ [10], [15] fulfilling

$$\psi(\rho, \theta + 2\pi/N) = e^{-j\frac{2\pi q}{N}} \psi(\rho, \theta) \quad (2)$$

where $N > 1$ is an integer determined by the geometry such that it is invariant to a $2\pi/N$ rad twist. The integer q is referred to as *mode class* [10], and, due to the periodicity of the complex exponential, can be defined in many ranges. However, it is common to take $[-N/2] < q \leq [N/2]$, since the modes with the same $|q|$ are degenerate [10]. C_N waveguides have N mode classes, one for each possible q value, as opposed to only two or four for the first-order symmetry case.

Second-order symmetries impose whether the first two modes of a structure are degenerate. Indeed, the first modes of a cross-section with second-order symmetry will be degenerate if the structure is at least C_N with $N \geq 3$ and belongs to the class $q = \pm 1$, regardless of the first-order symmetry (or the lack of it). This is proven directly by (2), since $N = 3$ is the lowest value for which the mode classes ± 1 exist. The mode in $q = 1$ is degenerate with the mode in $q = -1$, and they will be circularly polarized in the opposite direction.

C. Simultaneous First- and Second-Order Symmetry

When first- and second-order symmetries are present simultaneously, the structure is called $C_{N,\nu}$ [10], [15], and both first- and second-order symmetry properties are involved. In this case the mode classes $q = 0$ and $q = N/2$ are divided into two subclasses (noted as $q = 0 - \{A, B\}$ and $q = N/2 - \{A, B\}$). As a result, these cross-sections present $N + 1$ or $N + 2$ classes depending on the symmetry being one-fold or two-fold

TABLE I
SUMMARY OF SYMMETRIES AND MODE CLASSES

Symmetry Order	1 st	2 nd (C_N)	1 st & 2 nd ($C_{N,\nu}$)
Number of Classes	{2, 4}	N	$\{N + 1, N + 2\}$
Class Name	{A, B; A, B, C, D}	$[-N/2] < q \leq [N/2]$ –	$q = \{0-A, B;0, N/2-A, B\}$
Degen. 1 st Mode [†]	No [‡]		If $N \geq 3$
Class of 1 st Mode [†]	{B; C or D} [‡]		$q = \pm 1$
Scalable Unit Cell	No		Yes

Items between brackets refer to the first-order symmetry being either one-fold or two-fold.

[†]: In the full spectrum. [‡]: If the cross-section is not $C_{N,\nu}$ with $N \geq 3$.

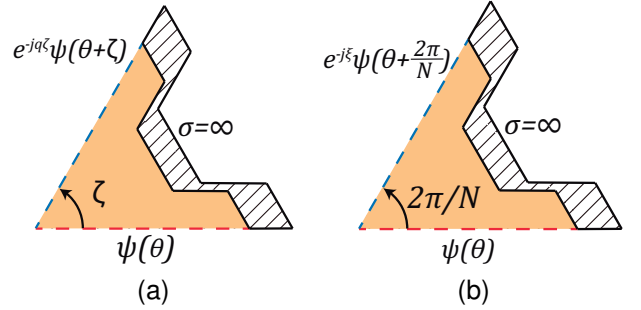


Fig. 2. Generic rotational unit cell that can be systematically scaled to any rotational symmetry factor N . (a) First test case, in which the angular width of the rotational unit cell is studied as a continuous parameter ζ and the mode class is fixed. (b) Second test case, in which the mode class is taken as a continuous parameter ξ and the geometry (angular width) is fixed.

[7]. Note that modes with $q \neq \{0, N/2\}$ will exhibit PEW and PMW simultaneously, on the real and imaginary part of the eigenfunction, respectively.

The properties regarding mode classes are briefly summarized in Table I, Note that only second-order symmetries have scalable rotational unit cells (in which N can be chosen to be arbitrary large), as opposed to the first-order symmetry case.

D. Mode Class Aliasing

When a cross-section is invariant to more than one value of N in (2), then it is possible to analyze it from multiple C_N perspectives. Let us consider two values $N_1 > N_2$ so that $N_1/N_2 = R$, where R is an integer. We can substitute the C_N constraint for the large wedge so that:

$$\psi(\rho, \theta + 2\pi/N_2) = e^{-j\frac{2\pi q_1 R}{N_1}} \psi(\rho, \theta) = e^{-j\frac{2\pi q_2}{N_2}} \psi(\rho, \theta). \quad (3)$$

Thus, we finally have that $q_1 = q_2 \bmod N_2 - [N_2/2]$ since $N_1 = RN_2$. Then, when considering two different multiples of N for a structure, the modes that belonged to certain classes are relocated to other classes, in what we introduce as *mode class aliasing*. Mode classes considering a wedge N_1 will be R times more populated in comparison to the analysis of the smaller wedge. This is analogous to considering one-fold first-order symmetry in a two-fold symmetric cross-section, which would relocate the modes from four classes into two.

Mode class aliasing may or may not have an effect on the bandwidth of each mode class, since the first higher-order

TABLE II
MODE-CLASS MONOMODE RELATIVE BANDWIDTH Δ (%) FOR A
CIRCULAR WAVEGUIDE WITH VARIOUS SYMMETRIC EXCITATIONS,
MODE CLASSES $q = \{0, \pm 1\}$

Excitation symmetry	$q = \pm 1$	$q = 0$	$q = 0\text{-A}$	$q = 0\text{-B}$
$C_3, C_{3,\nu}$	49.5	45.6	9.2	54.5
$C_4, C_{4,\nu}$	70.2	45.6	32.4	75.5
$C_5, C_{5,\nu}$	70.2	45.6	50.3	78.4
$C_6, C_{6,\nu}$	70.2	45.6	58.7	78.4
$C_\infty, C_{\infty,\nu}$	70.2	45.6	58.7	78.4

mode of each class might have a lower cutoff frequency than the aliased modes. Note that this behavior shows a consistency in terms of mode classes, since as many modes as possible remain in the same class regardless of the chosen analysis. Further discussion is presented in Section III-A.

III. MODAL SPECTRUM SHAPING AND CHARACTERIZATION OF THE ROTATIONAL UNIT CELL

Now we consider how increasing the symmetry factor N affects mode-class monomode relative bandwidth, defined as

$$\Delta = \frac{f'_c - f_c}{f_{mc}} \times 100(\%) \quad f_{mc} = \frac{f'_c + f_c}{2} \quad (4)$$

where f_c and f'_c are the cutoff frequencies of the first and second mode, respectively, of the class under study.

A. Effects of Mode Class Aliasing

To illustrate the behavior of mode class aliasing, we will consider a cross-section that can be analyzed from multiple C_N and $C_{N,\nu}$ perspectives. Although the reasoning can be applied to other C_N and $C_{N,\nu}$ geometries, we will use the circular waveguide for the discussion, whose mode classes are derived analytically in a very simple way in the Appendix. Moreover, in this case, since $N \rightarrow \infty$ mode class aliasing takes place for all possible N values. In this test, we have sought the minimum symmetry factor N of the excitation so that mode class aliasing does not influence the mode-class monomode relative bandwidth Δ .

In Table II, the mode-class monomode relative bandwidth Δ is presented for the circular waveguide studied for various rotational symmetry perspectives, from $N = 3$ to $N = 7$. Mode classes with more practical use $q = \{0, \pm 1\}$ were studied, for the former also considering $C_{N,\nu}$ symmetries ($q = 0\text{-}\{A,B\}$) separately. It was found that, as long as the excitation is at least C_4 , maximum bandwidth will be achieved for mode degenerate classes $q = \pm 1$. However, for mode class $q = 0$, a C_3 excitation already maximizes the bandwidth. When considering first-order symmetries as well as second-order symmetries, it is found that a C_4 excitation is enough to achieve maximum bandwidth for $q = 0\text{-B}$, while, for $q = 0\text{-A}$ a more strict C_6 excitation is needed. Note that, in general, Δ does not decrease as the symmetry factor increases. This is due to the nature of mode class aliasing: relocating the modes into an increasing amount of classes will make the superposition of modes into them stop being a limiting factor.

This information can be useful when designing devices with circular waveguide interfaces, because it shows that, as long

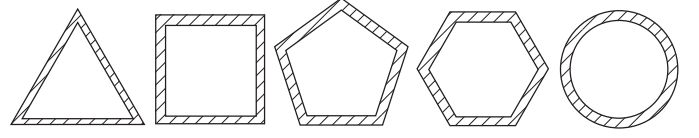


Fig. 3. Regular polygon waveguides with $C_{N,\nu}$ symmetry. Left-to-right: $N = 3, 4, 5, 6$, and ∞ sides.

TABLE III
FIRST $q = \pm 1$ TWO CUTOFF WAVENUMBERS k_c AND k'_c FOR THE
REGULAR POLYGONS IN FIG. 3 (NORMALIZED TO UNITY AREA).

Reg. polygon	C_3	C_4	C_5	C_6	C_∞
k_c	2.756	3.142	3.218	3.241	3.263 [†]
k'_c	5.512	7.025	6.914	6.863	6.792 [‡]
Δ (%)	66.7	76.4	73.0	71.7	70.2

[†]: k_c of the TE₁₁ modes. [‡]: k_c of the TM₁₁ modes.

TABLE IV
MODE-CLASS MONOMODE RELATIVE BANDWIDTH Δ (%) FOR VARIOUS
REGULAR POLYGONS (SHOWN IN FIG. 3) CONSIDERING DIFFERENT
SYMMETRY SCHEMES

Sym order	Class	3-side	4-side	5-side	6-side	∞ -side
1 st	A	53.5	34.0	46.2	23.8	23.8
1 st	B	53.5	34.0	29.1	23.8	23.8
1 st	C	-	76.4	-	71.7	70.2
1 st	D	-	76.4	-	71.7	70.2
2 nd	0	0	34.0	42.0	43.8	45.6
2 nd	± 1	66.7	76.4	73.0	71.7	70.2
2 nd	± 2	-	34.0	37.4	52.9	50.8
2 nd	± 3	-	-	-	17.4	40.6
1 st & 2 nd	0-A	53.5	34.0	43.1	53.5	58.7
1 st & 2 nd	0-B	53.5	76.2	77.7	78.1	78.4
1 st & 2 nd	$N/2\text{-A}$	-	76.2	-	53.5	-
1 st & 2 nd	$N/2\text{-B}$	-	34.0	-	31.9	-

as the device and the excitation are both at least C_4 (i.e. C_N with $N \geq 4$), maximum bandwidth can be achieved for the first mode for mode class $q = \pm 1$.

B. Maximizing Bandwidth for a Rotational Unit Cell

To comprehend how the symmetry factor N influences mode-class monomode relative bandwidth Δ , we will consider waveguides defined by regular polygons. This case is a good starting point, since asymptotic results are available (see the Appendix). Table III shows the first cutoff wavenumbers for various regular polygons obtained by [15] with a cross-section normalized to unity area. The k_c values (whose actual dimension is the inverse of length) and the dimensions defining the geometries are normalized (unitless) from now on.

In Table IV, the value of (4) is given for regular polygons of $N = 3, 4, 5, 6$, and ∞ sides. In second-order symmetry they are labeled depending on their mode class q , and, in the combination of both, $q = 0$ and $q = N/2$ are subdivided into two classes combining the nomenclatures of both previous schemes. Note that classes $q = \pm 1, \pm 2$, etc. also exist for $C_{N,\nu}$ but they are not shown due to being identical as the C_N case. In the C_∞ case, in the last two rows, $N/2$ cannot be evaluated since N tends to infinity.

The highest bandwidth (76.2 %) of a degenerate mode class (i.e. for $q \neq \{0, N/2\}$) is obtained for the square waveguide

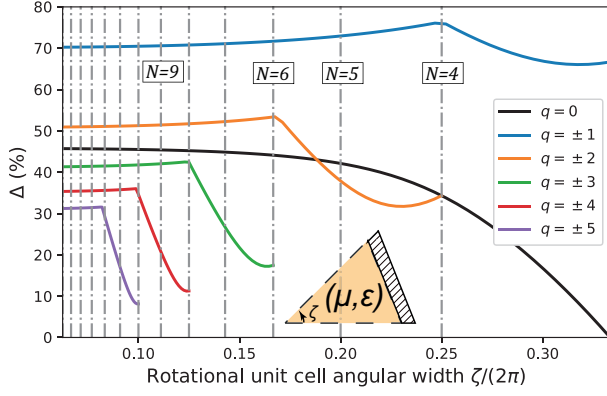


Fig. 4. Mode-class monomode relative bandwidth Δ against angular width $\zeta/(2\pi)$ for the modes associated to the displayed rotational unit cell, according to the problem in Fig 2(a). Vertical lines indicate physically feasible values (i.e. when $N = 2\pi/\zeta$ is an integer), that lead to a regular polygon.

and two-fold or a C_4 symmetry; while the highest Δ for the entire analysis is obtained in $q = 0$ —B for a circular waveguide (78.4 %), justifying the choices presented in Table II.

The values of Table IV seem to indicate that a relationship can be found for the mode class monomode bandwidth between regular polygons in the context of rotational (second-order) symmetry. To test this hypothesis, we can consider wedges with arbitrary values for its angular width ζ , so that the boundary condition from (2) is now replaced by

$$\psi(\rho, \theta + \zeta) = \psi(\rho, \theta)e^{-jq\zeta} \quad (5)$$

as shown in Fig. 2(a). The method from [15] is used to obtain the modes associated to the rotational unit cell, using (5) instead of (2). This variable change allows for the analysis shown in Fig. 4, where it is found that, in this case, all the functions with $q \neq 0$ have a maximum. Nevertheless, this maximum does not necessarily occur for realizable polygons and could not be observed without this analysis (only the rotational unit cells in which $2\pi/\zeta$ becomes an integer N are physically feasible, marked in Fig. 4 with vertical dashed lines, which correspond to the values in Table IV for the rows with second-order symmetry).

Another rotational unit cell is analyzed as proposed in Fig. 5. We can also observe a decreasing mode class monomode bandwidth as the mode class increases from $|q| = 1$. However, the maxima are not achieved for the same $N = 2\pi/\zeta$. This indicates that, given a rotational unit cell, a polygon with a set number of sides can be sought to find advantageous geometries. Note that this theory also performs with fictitious (non-integer) mode classes \tilde{q} . For example $\tilde{q} = \pm 1.5$, as shown in dashed lines in Fig. 5, presents values between $q = \{1, 2\}$.

C. Understanding the Effect of the C_N Constraint in Mode Class Bandwidth and the Relationship Between Mode Classes

The C_N constraint gives a set of modes via fixing the phase between two boundaries angularly separated $2\pi/N$ rad. If we define a geometry (N is fixed), we can consider the phase difference not as an exact multiple of this quantity, but as a continuous function, as shown in Fig. 2(b):

$$\psi(\rho, \theta + 2\pi/N) = \psi(\rho, \theta)e^{-j\xi}. \quad (6)$$

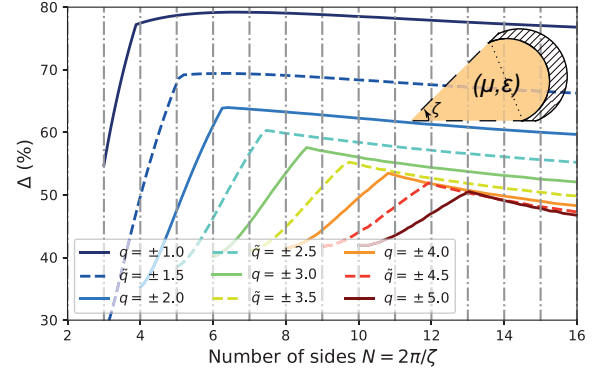


Fig. 5. Mode-class monomode relative bandwidth Δ against the symmetry factor $N = 2\pi/\zeta$ for the displayed rotational unit cell. Vertical lines indicate physically feasible values.

Now, we can again use [15], replacing (2) by (6), to characterize the modes associated to this rotational unit cell. This concept differs from the one in Section III-B in the sense that, in this case, the geometry does not vary. It leads to a rotational transversal dispersion diagram, analogous to a Brillouin zone, which is then sampled at the real (non-fictitious) phase differences. The correspondence to true mode classes is defined by the possible values of q where $\xi/(2\pi) = q/N \leftrightarrow \xi = 2\pi q/N$. This way, we can appreciate the effect of the rotational symmetry constrain on spectrum shaping, obtaining what we introduce as *supermode curves* in the rotational unit cell. These curves will translate into N true C_N modes ($[-N/2] < q \leq [N/2]$) when sampling each curve. The concept of supermode curves is further justified when considering that modes are equally distributed between classes [15]. Hence, for N modes of each class, we have one smooth dispersion curve to be sampled at N points.

In Fig. 6, the first 6 supermode curves (noted as TE_i^{sm} and TM_i^{sm} , $i = 0, 1, \dots$) are shown for a square waveguide ($C_{4,\nu}$). To obtain the C_N modes, this diagram is sampled at the vertical lines, denoted in a black discontinuous line. The orange and green line, belonging to TE_0^{sm} TM_0^{sm} , respectively, cross exactly at $\xi/(2\pi) = \pm 1/4 = q/N$ ($q = \pm 1$). Indeed, at this point they become combinations with complex amplitudes in quadrature of the well-known modes in a square waveguide with linear polarization: $TE_{21} \pm jTE_{12}$ and $TM_{21} \pm jTM_{12}$, which have the same cutoff frequency, as expected.

In Fig. 7(a), the same diagram was obtained for the $C_{4,\nu}$ cross-section designed with the rotational unit cell geometry in Fig. 5 with $r = 1$. The curves have slightly changed, and the orange and green line no longer cross each other at $\xi/(2\pi) = \pm 1/4$. These lines clearly denote a geometry-dependent relationship between supermode curves which could not be observed without this analysis. Finally, in Fig. 7(b), the first supermode curves for the same rotational unit cell as in Fig. 7(a), but in this case scaling it to C_5 . We can see that the supermode curves are fairly similar. However, in this case, true (non-fictitious) modes lie in the sampling points $\xi/(2\pi) = 0, \pm 1/5$, and $\pm 2/5$.

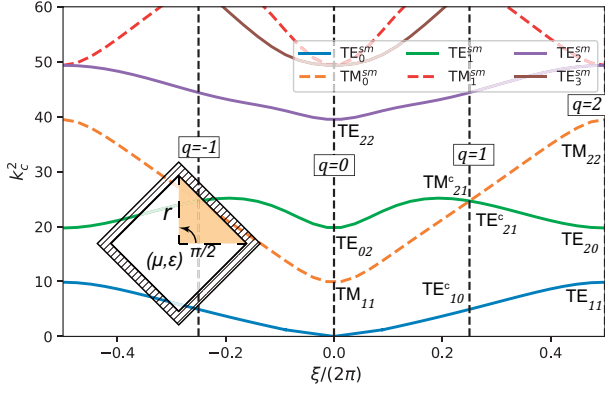


Fig. 6. Rotational transversal dispersion diagram (according to Fig. 2(b)) for the first six supermode curves in a C_4 ($q = \{-1, 0, 1, 2\}$) regular polygon with $r = 1$. Dashed black lines represent the verticals corresponding to the true mode classes, i.e., the values intersected by those lines belong to the modes of the waveguide. Modes have been noted with classic indexing [16] in the intersections, although the superscript c indicates that the mode is a linear combination with quadrature amplitudes as: $\text{TE}_{mn}^c = \text{TE}_{mn} \pm j\text{TE}_{nm}$ and $\text{TM}_{mn}^c = \text{TM}_{mn} \pm j\text{TM}_{nm}$.

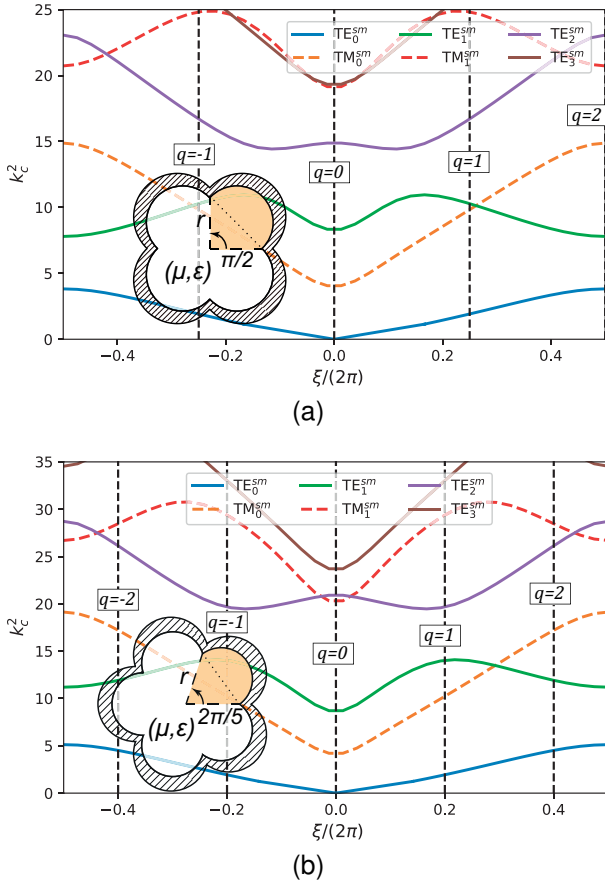


Fig. 7. Rotational transversal dispersion diagram (according to the problem in Fig. 2(b)) for the first supermode curves in a cross-section obtained with the rotational unit cell in Fig. 5 ($r = 1$): (a) $N = 4$ ($q = \{-1, 0, 1, 2\}$), (b) $N = 5$ ($q = \{-2, -1, 0, 1, 2\}$). Dashed black lines represent the verticals corresponding to the true mode classes, i.e., the values intersected by those lines belong to the modes of the waveguide.

IV. PROPOSED WORKFLOW

In this final section we will use the all presented tools to design a simple ridged circular waveguide intended for dual

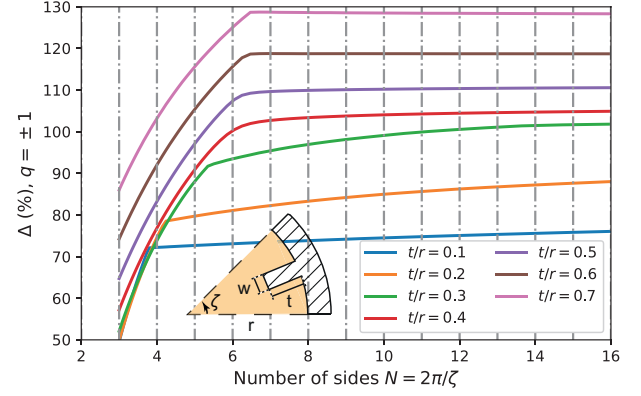


Fig. 8. Mode-class monomode relative bandwidth Δ for $q = \pm 1$, for the cross-section shown in the inset with normalized dimensions $r = 0.1$, $t = 0.5r$, $w = 0.1/N$.

polarization working with its first two degenerate modes (i.e. mode class $q = \pm 1$). We will first consider the effect on varying the length of the ridges against the radius of the circle t/r (see the inset in Fig. 8), while defining the width of the ridges as $w = 0.1\zeta/(2\pi)$, so that the rotational unit cell can scale to arbitrary values of N . As it can be seen in Fig. 8, obtained through (5) and the theory in Section III-B, for the $q = 1$ case the mode-class monomode relative bandwidth is monotonously increasing for this class with the ridged cross-section as we increase the symmetry factor N . However, after a certain point, the benefits of adding more ridges becomes less useful. Thanks to considering non-integer unit cells we can see that, for a large t/r , the knee-like effect appears at around $N = 6$. Since, in practice, the excitation becomes more complex as N increases, a good compromise seems to be $t/r = 0.5$ and $N = 6$, which gives a mode-class monomode relative bandwidth of 107.7 %. In a more realistic application, the smallest N value that achieves the desired Δ would be chosen, while considering how other parametric variations shape the proposed diagrams.

After selecting the geometry, we check if it is possible for our geometry to have a simpler excitation, given the theory from Section II-D. With the initial parameters $r = 0.1$ and $w = 0.1/N$, the first mode for the full spectrum has a cutoff wavenumber of $k_c = 14.74$. If we consider two-fold first-order symmetry, we find that class D has $k'_c = 49.14$ as the first higher-order cutoff wavenumber. However, class C has a higher-order mode at $k'_c = 19.44$ due to the rotational unit cell not having first-order symmetry itself. Since both classes are needed for dual polarization, the system will be limited by class C. If we check the propagation of the structure with C_3 excitation we obtain that the first higher-order mode of classes $q = \pm 1$ has a $k'_c = 18.52$. Finally, with C_6 excitation, the second cutoff wavenumber for classes $q = \pm 1$ is at $k'_c = 49.14$. We can conclude that, in this case, the excitation for the proposed design must necessarily be at least C_6 . This analysis is summarized in Table V.

We will finally consider the effect of modifying the width of the ridges by using the diagrams described in Section III-C, as supermode curves can help in visually showing the behavior

TABLE V
 k_c AND k'_c OF FIG. 9 (INSET). $r = 0.1$, $t/r = 0.5$, $w = 0.1/6$
 CONSIDERING VARIOUS SYMMETRY SCHEMES.

Sym. order	1 st , 2-fold	1 st , 2-fold	2 nd , $N = 3$	2 nd , $N = 6$
Class	C	D	$q = \pm 1$	$q = \pm 1$
k_c	14.74	14.74	14.74	14.74
k'_c	19.51	49.14	18.52	49.14
Δ (%)	27.85		22.73	107.7

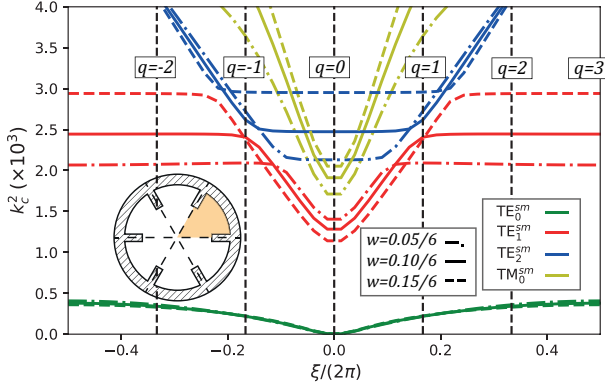


Fig. 9. Rotational transversal dispersion diagram (according to the problem in Fig. 2(b)) for the first C_6 supermode curves for the figure in the inset with $r = 0.1$, $t = 0.5r$.

of parametric variations close to sampling points of interest. In Fig. 9 supermode curves are shown for various widths $w = \{0.05, 0.1, 0.15\}/6$, corresponding, respectively, to the dash-dotted, solid and dashed lines. We can observe that, in this cross-section TM_0^{sm} (yellow) is above TE_1^{sm} (red). As w is increased, the dispersion curve of TE_0^{sm} barely changes, while the valley of TE_1^{sm} becomes larger. After a certain point, we are no longer obtaining a better ratio at the sampling point $\xi/(2\pi) = \pm 1/6$. Thus, in this case, we can assume that ridges with $w \geq 0.1/6$ will provide an optimal solution. In a more realistic case, mechanical specifications would also play a key role in this analysis.

V. CONCLUSION

In this work we have addressed the problem of spectrum shaping in waveguides with first- and/or second-order symmetric cross-sections using the concept of rotational mode classes. It has been found that the presented approach, where the rotational unit cell plays a key role, can aid in the design of waveguide cross-sections. Rotational transversal dispersion diagrams also provide a better understanding of the effect of the C_N boundary conditions, mode class control, and the effect of the design parameters in the modal spectrum shaping.

APPENDIX

ASYMPTOTIC VALUES FOR REGULAR POLYGONS

We can analytically derive the rotationally symmetric modes of each class for the circular (C_∞) waveguide directly with the C_N constraint, which is the limit case for regular polygons. If we consider the variable separation $\psi = r(\rho)s(\theta)$ we can rewrite the Helmholtz equation, as done in classical texts [16]:

$$\rho^2 \frac{d^2 r(\rho)}{d\rho^2} + \rho \frac{dr(\rho)}{d\rho} + \rho^2 k_c^2 r(\rho) = \frac{-d^2 s(\theta)}{s(\theta) d\theta^2}. \quad (7)$$

It can be seen that the solution for $s(\theta)$ can be chosen simply as $s(\theta) = e^{-jk_\theta\theta}$, where k_θ is a constant. Now let us consider the function s at a small angular distance δ_θ with respect to the reference θ :

$$s(\theta + \delta_\theta) = e^{-jk_\theta(\theta + \delta_\theta)} = e^{-jk_\theta\delta_\theta} s(\theta). \quad (8)$$

Since we know from (2) that $\psi(\rho, \theta + \zeta) = e^{-j\zeta q} \psi(\rho, \theta)$, then, we come to the conclusion that $k_\theta = q$. Since q is an integer, this result also fulfills the continuity condition $s(\theta + 2\pi) = s(\theta)$. Finally, by substituting this result into (7), we arrive at the class-dependent expression for the C_N modes in the circular waveguide (when studied as a C_∞), which, as expected, is consistent with the classical derivation [16]:

$$\psi = J_q(k_c \rho) e^{-jq\theta} \quad k_{c,TE} = \frac{p'_{m,q}}{r} \quad k_{c,TM} = \frac{p_{m,q}}{r} \quad (9)$$

where $p_{m,q}$, $p'_{m,q}$ are the m th zeroes of the q th order Bessel function J or its derivative, respectively. Importantly, in (9), the value of q determines the mode class of the complex-valued eigenfunction ψ .

REFERENCES

- [1] M. Dohler, E. Okon, W. Malik, A. Brown, B. Allen, and D. Edwards, *Ultra-Wideband Antennas and Propagation: For Communications, Radar and Imaging*. John Wiley & Sons, 2006.
- [2] W. Jiang, B. Han, M. A. Habibi, and H. D. Schotten, "The road towards 6G: A comprehensive survey," *IEEE Open J. Commun. Soc.*, vol. 2, pp. 334–366, 2021.
- [3] A. Goldsmith, *Wireless communications*. Cambridge, UK: Cambridge university press, 2005.
- [4] J. L. Volakis, *Antenna engineering handbook*. New York, NY, USA: McGraw-Hill Education, 2007.
- [5] W. Wang, S.-S. Zhong, Y.-M. Zhang, and X.-L. Liang, "A broadband slotted ridge waveguide antenna array," *IEEE Trans. Antennas Propag.*, vol. 54, no. 8, pp. 2416–2420, 2006.
- [6] O. B. Jacobs, J. W. Odendaal, and J. Joubert, "Quad-ridge horn antenna with elliptically shaped sidewalls," *IEEE Trans. Antennas Propag.*, vol. 61, no. 6, pp. 2948–2955, 2013.
- [7] M. Mrozowski, *Guided Electromagnetic Waves: Properties and Analysis*. Badlock, UK: Research Studies Press Ltd., 1997, vol. 3.
- [8] J. Uher, J. Bornemann, and U. Rosenberg, *Waveguide Components for Antenna Feed Systems: Theory and CAD*. Norwood, MA, USA: Artech House Antenna Library, 1993.
- [9] G. Conciauro, *Advanced Modal Analysis: CAD Techniques For Waveguide Components and Filters*. John Wiley & Sons, 2000.
- [10] P. McIsaac, "Symmetry-induced modal characteristics of uniform waveguides - II: Theory," *IEEE Trans. Microw. Theory Techn.*, vol. 23, no. 5, pp. 429–433, 1975.
- [11] A. A. Kirilenko, S. O. Steshenko, V. N. Derkach, and Y. M. Ostryzhnyi, "A tunable compact polarizer in a circular waveguide," *IEEE Trans. Microw. Theory Techn.*, vol. 67, no. 2, pp. 592–596, 2019.
- [12] N. Kolmakova, S. Prikolotin, A. Perov, V. Derkach, and A. Kirilenko, "Polarization plane rotation by arbitrary angle using D_4 symmetrical structures," *IEEE Trans. Microw. Theory Techn.*, vol. 64, no. 2, pp. 429–435, 2016.
- [13] O. Dahlberg, R. Mitchell-Thomas, and O. Quevedo-Teruel, "Reducing the dispersion of periodic structures with twist and polar glide symmetries," *Sci. reports*, vol. 7, no. 1, pp. 1–6, 2017.
- [14] O. Zetterstrom, G. Valerio, F. Mesa, F. Ghasemifard, M. Norgren, and O. Quevedo-Teruel, "Mode-matching analysis of loaded transmission lines with twist symmetries," in *2020 14th Eur. Conf. Antennas Propag. (EuCAP)*, 2020, pp. 1–5.
- [15] G. Garcia-Contreras, J. Córcoles, and J. A. Ruiz-Cruz, "Rigorous modal characterization of first- and second-order symmetric waveguides using specular periodic boundary conditions in 2D-FEM," *IEEE Trans. Antennas Propag.*, vol. 70, no. 11, pp. 10 800–10 810, 2022.
- [16] R. E. Collin, *Field Theory of Guided Waves*. Piscataway, NJ, USA: John Wiley & Sons, IEEE Press, 1990.